Applied Physics Letters

RESEARCH ARTICLE | OCTOBER 23 2026

Scanning gate microscopy modulation of supercurrent in graphene Josephson junctions

Ivan Villani ; Samuele Fracassi ; Niccolò Traverso Ziani ; Maura Sassetti ; Matteo Carrega ; Vaidotas Mišeikis ; Camilla Coletti ; Fabio Beltram ; Kenji Watanabe ; Takashi Taniguchi ; Sergio Pezzini ; Stefan Heun

Check for updates

Appl. Phys. Lett. 129, 162601 (2026)
https://doi.org/10.1063/5.0354810

View Online
Export Citation

Articles You May Be Interested In

Anomalous supercurrent and diode effect in locally perturbed topological Josephson junctions

Appl. Phys. Lett. (June 2024)

Long-range triplet supercurrents induced by singlet supercurrents parallel to magnetic interfaces

Appl. Phys. Lett. (November 2014)

Long range supercurrents in ferromagnetic CrO_2 using a multilayer contact structure

Appl. Phys. Lett. (February 2012)

23 October 2026 16:18:24



AIP Publishing

Applied Physics Letters ARTICLE pubs.aip.org/aip/apl

Scanning gate microscopy modulation of supercurrent in graphene Josephson junctions

Cite as: Appl. Phys. Lett. **129**, 162601 (2026); doi: 10.1063/5.0354810
Submitted: 31 July 2026 · Accepted: 6 October 2026 ·
Published Online: 23 October 2026

View Online Export Citation CrossMark

Ivan Villani,[1] Samuele Fracassi,[2,3] Niccolò Traverso Ziani,[2,3] Maura Sassetti,[2,3] Matteo Carrega,[3] Vaidotas Mišeikis,[4] Camilla Coletti,[4] Fabio Beltram,[1] Kenji Watanabe,[5] Takashi Taniguchi,[6] Sergio Pezzini,[1,a)] and Stefan Heun[1,b)]

AFFILIATIONS

[1]Istituto Nanoscienze–CNR, NEST-Scuola Normale Superiore, Piazza San Silvestro 12, 56127 Pisa, Italy
[2]Dipartimento di Fisica, Università di Genova, Genova, Italy
[3]CNR-SPIN, Via Dodecaneso 33, 16146 Genova, Italy
[4]Center for Nanotechnology Innovation, Laboratorio NEST, Istituto Italiano di Tecnologia, 56127 Pisa, Italy
[5]Research Center for Electronic and Optical Materials, National Institute for Materials Science, 1-1 Namiki, Tsukuba 305-0044, Japan
[6]Research Center for Materials Nanoarchitectonics, National Institute for Materials Science, 1-1 Namiki, Tsukuba 305-0044, Japan

[a)]**Electronic mail:** sergio.pezzini@cnr.it
[b)]**Author to whom correspondence should be addressed:** stefan.heun@cnr.it

ABSTRACT

Graphene Josephson junctions (JJs) represent an excellent platform for quantum technologies, thanks to the combination of high carrier mobility, ballistic transport, and gate-tunable critical currents, preserved even under quantizing magnetic fields. Investigating the spatial distribution of supercurrent flow could be crucial for elucidating transport mechanisms and advancing the engineering of these devices. In this work, we employ a scanning gate microscope to investigate supercurrent transport in hexagonal boron nitride-encapsulated graphene JJs. We study the supercurrent modulation as a function of tip voltage bias and tip-to-sample distance and provide a complete characterization of the tip-induced modulation. Our experimental results are quantitatively consistent with numerical simulations and pave the way toward local mapping and manipulation of gate-tunable superconducting phenomena with unprecedented spatial resolution.

© 2026 Author(s). All article content, except where otherwise noted, is licensed under a Creative Commons Attribution (CC BY) license (https://creativecommons.org/licenses/by/4.0/). https://doi.org/10.1063/5.0354810

23 October 2026 16:18:24

The proximity effect induces superconductivity in a normal weak link inserted between two superconducting leads, forming a Josephson junction (JJ).[1] Nowadays, JJs serve as key elements for a wide range of quantum technologies and superconducting devices.[2–11] Utilizing field-effect-tunable materials such as graphene as the weak link enables gate control of the superconducting properties.[12–17] JJs based on graphene (GJJs) encapsulated in hexagonal boron nitride (hBN) stand out for their large supercurrent densities, high interface transparency, and ballistic transport over micrometer-scale.[18,19] These features enable enticing new capabilities, such as the proximity effect in the quantum Hall regime,[20–25] a promising path toward the realization of hardware for topological quantum computation.[26–29]

Traditionally, the characterization of JJs relies on electrical transport measurements. While this approach provides valuable information on a macroscopic scale, it prevents access to spatially resolved information. Scanning gate microscopy (SGM) has emerged as a powerful technique for spatial mapping of electrical transport in gate-tunable materials. This technique is based on a voltage-biased conductive tip of an atomic force microscope (AFM) that can be employed as a movable local gate. By measuring how the tip affects the conductance of the device, one can infer the transport properties on the local scale. Pioneering work employing SGM has been performed by Topinka *et al.*[30–34] Subsequently, SGM has been employed on semiconductors,[35,36] quantum wells,[37] two-dimensional electron gases (2DEGs),[38–40] quantum dots,[41] and graphene.[42–45] In combination with a magnetic field, SGM enabled imaging of electron trajectories[46] in 2DEGs[47] and in graphene.[48,49] The technique has also been employed in the quantum Hall regime.[50–54]

Since the critical current of GJJs is gate-tunable,[18] SGM appears as a powerful tool for the spatial investigation of local transport

© Author(s) 2026

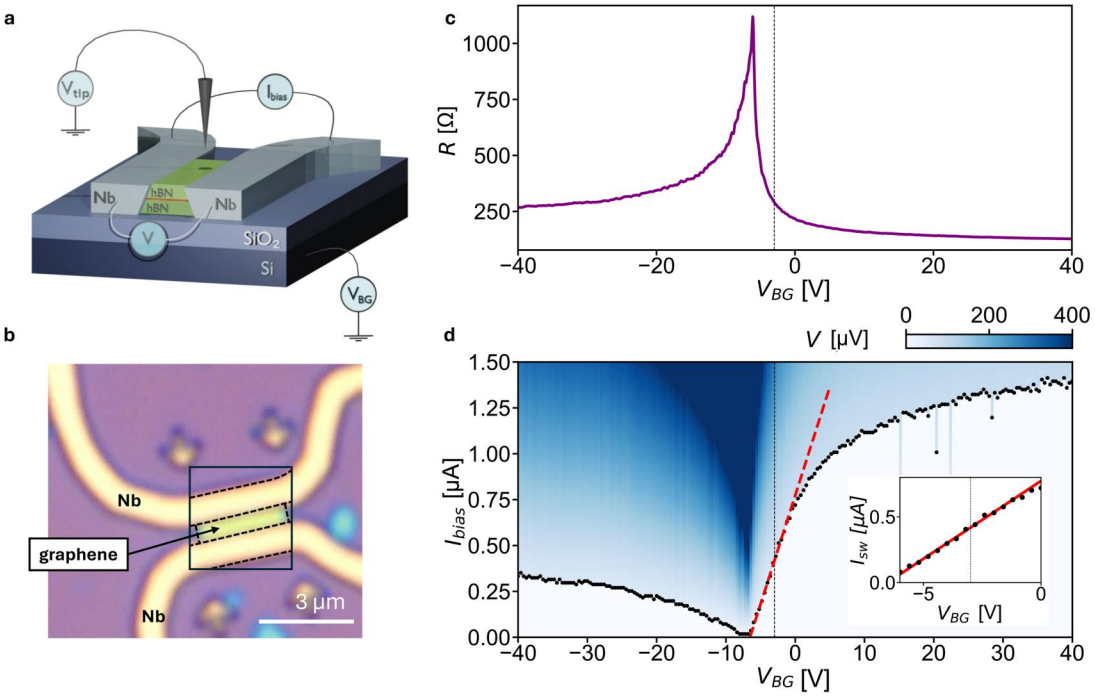


FIG. 1. (a) Schematics of sample geometry and SGM setup. Graphene is encapsulated in hexagonal boron nitride (hBN) and contacted by niobium (Nb) leads. A bias V_{tip} is applied to the tip, which scans above the sample at fixed distance. A bias V_{BG} is applied to the back-gate. A current I_{bias} is applied to the junction, and the voltage drop V is measured. (b) Optical microscopy image of junction J1 ($W = 3\,\mu$m and $L = 600$ nm). The black square indicates the scanning area of SGM maps shown in Fig. 2. The black dashed lines outline the junction structure. (c) Back-gate sweep measured with a lock-in amplifier by applying a 100 nA AC bias. The temperature is set to $T = 2.7$ K to obtain the normal-state resistance R. The vertical dashed line indicates the working point for the analysis presented in Fig. 2, at $V_{BG} = -3$ V. (d) Voltage drop as a function of back-gate voltage V_{BG} and DC current bias I_{bias}. The sweep direction is from 0 to finite current values. The white region of zero voltage drop identifies the supercurrent branch. The switching current, extracted by setting a threshold of 1.5 μV on the measured voltage drop, is indicated by black dots. The dashed red line is a linear fit to I_{sw} across the working point, used to determine the back-gate switching current modulation efficiency, $\beta_{BG,n} = 118 \pm 3$ nA/V. (*Inset*) Switching current in a ± 3 V range around the working point. The dependence of $I_{sw}(V_{BG})$ can be approximated as linear.

properties in the superconducting regime. This potential recently inspired theoretical efforts to model the effect of an SGM tip on the induced superconductivity.[55–57] However, on the experimental side, only a handful of SGM experiments have been reported on superconducting devices.[58–61] Huefner *et al.* used SGM to characterize superconducting single electron transistors,[58] Hegedüs *et al.* employed SGM to study the nature of two-level system defects in qubits,[59] and Bhandari *et al.* imaged Andreev reflections at a single graphene–superconductor interface.[60] Lombardi *et al.*[61] represents the first example of application of SGM to JJs. A switching current modulation of a few nA was reported in an InSb nanoflag JJ, setting an important proof-of-concept for investigating supercurrent modulation in this class of devices.

Here, we employ SGM to investigate the supercurrent modulation in hBN-encapsulated GJJs. Thanks to large switching currents and a geometry that is particularly suitable for SGM investigation, we obtain a large tip-induced modulation of hundreds of nA. We study the tip-induced supercurrent modulation as a function of tip voltage (at fixed tip height) and of tip-to-sample distance. A theoretical model supporting our experimental results is also reported. We provide a complete characterization of the tip-induced modulation of the critical current. This work thus identifies GJJs as the ideal platform for imaging supercurrent transport with unprecedented spatial resolution.

SGM measurements were performed at a base temperature of 300 mK. The sample is mounted on an Attocube AFM head attached to the ^{3}He pot of a Janis cryostat. The AFM–SGM tip is mounted on a tuning fork and is electrically connected to a voltage source that controls the tip voltage bias V_{tip}. All electrical lines, including the connections to the AFM components, are equipped with cryogenic filters. A sketch of the device layout and measurement configuration is shown in Fig. 1(a). Graphene is encapsulated in two 30 nm thick hBN flakes, resulting in a total stack thickness of 60 nm. The stack is released onto a Si/SiO_2 wafer (300 nm oxide thickness) that acts as a back-gate. Niobium (Nb) edge-contacts are obtained by DC magnetron sputtering performed after dry etching of the hBN–graphene–hBN stack. The thickness of the Nb contacts was conveniently set to match the height of the stack, to avoid height differences on the surface of the devices. We employ graphene single crystals grown by chemical vapor deposition[62] that guarantee electrical transport properties comparable to state-of-the-art exfoliation-based samples.[63] Further details on the sample layout are presented in the supplementary material. The investigated sample comprises two JJs of different length L and width W. Junction J1 has $L = 600$ nm and $W = 3\,\mu$m, and junction J2 has

23 October 2026 16:18:24

© Author(s) 2026

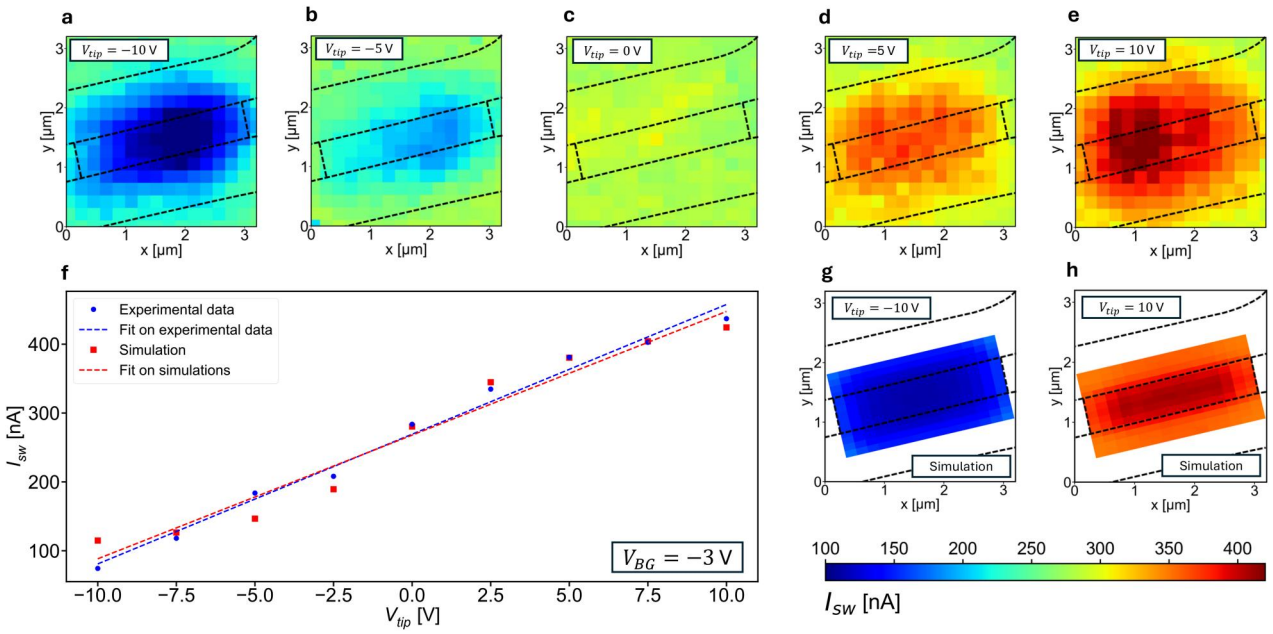


FIG. 2. (a)–(e) SGM maps of I_{sw} in the electron doping regime ($V_{BG} = -3$ V), for different values of V_{tip}. Black dashed lines outline the junction geometry. (f) Critical current modulation as a function of V_{tip}. Experimental points [extracted from SGM maps as in (a)–(e)] and best fit are shown in blue: $\beta_{tip,n} = 18.8 \pm 0.8$ nA/V. Results of numerical simulations are shown in red and are in excellent agreement with experimental data: $\beta_{simul,n} = 18.0 \pm 1.4$ nA/V. (g) Simulation of the SGM map in (a), for $V_{tip} = -10$ V. (h) Simulation of the SGM map in (e), for $V_{tip} = 10$ V. Same color scale for experimental data and simulations. Junction J1, $T = 300$ mK, $d = 100$ nm.

$L = 800$ nm and $W = 4\,\mu$m. The two JJs are in the long to intermediate ballistic regime and exhibit comparable transport properties, both in the normal state and in the superconducting regime.

An optical microscopy image of junction J1 is shown in Fig. 1(b) (to avoid damage to the GJJs that occurred in test experiments, no AFM topographic images were acquired during this experiment). The normal-state resistance of J1 is modulated by the back-gate voltage (V_{BG}) as shown in Fig. 1(c). Maximum resistance is observed at the charge neutrality point (CNP), which is shifted toward negative V_{BG} as a result of the induced doping by the Nb contacts. In junction J1, $V_{BG}^{CNP} = -6.3$ V, similar to previous devices fabricated using the same protocol.[11,23] The resistance approaches its minimum value to the right of the CNP, $V_{BG} > V_{BG}^{CNP}$, in the electron doping regime. For $V_{BG} < V_{BG}^{CNP}$, in the hole doping regime, the resistance is always larger due to p–n barriers originating from Fermi level pinning at the Nb–graphene interfaces.[18,19,23] The induced supercurrent is also modulated by the back-gate voltage, as illustrated in Fig. 1(d), where we report the voltage drop V across J1 as a function of V_{BG} and DC current bias I_{bias}. In these measurements, I_{bias} is swept from 0 to finite values. The supercurrent branch corresponds to the white region of zero voltage drop, and the switching current I_{sw}, extracted by setting a threshold of 1.5 μV on the measured voltage drop V, is indicated by the black dots. I_{sw} is maximum for large electron doping, lower on the hole doping side, and minimum at CNP. Overall, the switching current shows a non-linear dependence on V_{BG}. A convenient choice for SGM investigation is a working point with a large I_{sw}, combined with a linear $I_{sw}(V_{BG})$ dependence with a large slope. The working point was set to $V_{BG} = -3$ V, in the electron doping regime, indicated in Fig. 1(c) by the black dashed line. At this working point, the number of propagating modes (for each spin and valley degree of freedom) is equal to $N = 75$. The corresponding interface transparency is $Tr = 0.5$, calculated following Ref. 19. Performing a linear fit to $I_{sw}(V_{BG})$ across the working point [red dashed line in Fig. 1(d)], we obtain a back-gate modulation efficiency $\beta_{BG,n} = 118 \pm 3$ nA/V. $I_{sw}(V_{BG})$ is well approximated by this linear dependence [inset to Fig. 1(d)].

In Fig. 2, we investigate the switching current modulation vs V_{tip} of junction J1. The tip is scanned in vacuum above the junction at a fixed distance of $d_{vac} = 70$ nm from the top surface. Given the thickness of the top hBN flake $d_{hBN} = 30$ nm, the distance between the tip and the graphene channel is $d = d_{vac} + d_{hBN} = 100$ nm. In Figs. 2(a)–2(e), we report SGM maps of I_{sw} as a function of tip position for different V_{tip} values, ranging from −10 to +10 V. Maps are acquired by defining a grid over an area of $3.2 \times 3.2\,\mu$m^2 [continuous black square in Fig. 1(b)]. A V–I_{bias} curve is measured at each pixel of the grid, by sweeping the DC bias from 0 to finite values, and I_{sw} is extracted with the same criterion as in Fig. 1(d), by setting a threshold on the measured voltage drop. The obtained values are then plotted as a function of x–y position. Black dashed lines outline the junction geometry. We observe a reduction of the switching current for negative V_{tip}, while we observe an enhancement for positive V_{tip}. This is consistent with a positive back-gate modulation coefficient $\beta_{BG,n} > 0$: in the electron doping regime, supercurrent is enhanced (reduced) as the back-gate voltage is increased (reduced). Furthermore, the switching current variation is larger as $|V_{tip}|$ is increased. For $V_{tip} = -10$ V, we observe the maximum switching current reduction [Fig. 2(a)]. The reduction gets weaker for $V_{tip} = -5$ V [Fig. 2(b)] and becomes negligible at $V_{tip} = 0$ V [Fig. 2(c)]. For positive V_{tip}, the switching current

23 October 2026 16:18:24

© Author(s) 2026

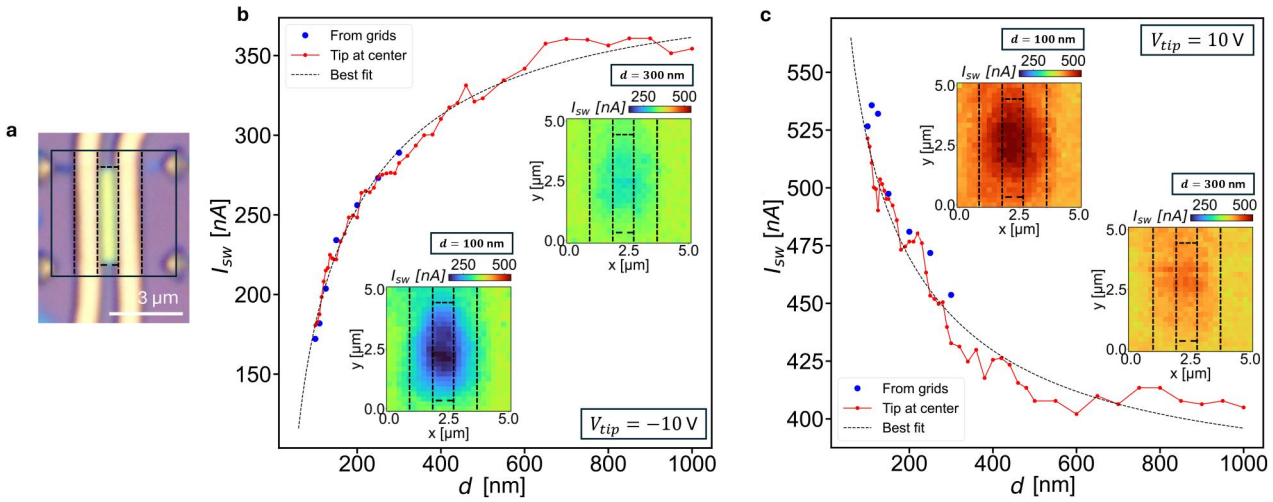


FIG. 3. (a) Optical microscopy image of junction J2. The black square indicates the scanning area for SGM maps. Dashed black lines outline the device geometry. (b) and (c) I_{sw} as a function of distance d between tip and graphene channel in the electron doping regime ($V_{BG} = -3$ V). $V_{tip} = -10$ V in (b); $V_{tip} = 10$ V in (c). Best fits to red dots using Eq. (1) are plotted as dashed black lines. 5×5 μm^2 SGM maps of I_{sw}, for $d = 100$ and 300 nm, are presented in the insets. Same color scale for all four images. Junction J2, $T = 300$ mK.

is enhanced, and a larger increase is reported in Fig. 2(e) ($V_{tip} = 10$ V) compared to Fig. 2(d) ($V_{tip} = 5$ V). In each map, the maximum modulation is observed when the tip is located over the junction and decreases when the tip is moved away.

In Fig. 2(f), we show the maximum switching current modulation extracted from each SGM map as blue dots (data acquired with the tip held fixed over the junction center are reported in the supplementary material). For the switching current value at $V_{tip} = 0$ V, we consider the average value over the entire map in Fig. 2(c). We obtain the tip modulation efficiency from a linear fit to $I_{sw}(V_{tip})$ [blue dashed line in Fig. 2(f)] as $\beta_{tip,n} = 18.8 \pm 0.8$ nA/V, equal to $16 \pm 1\%$ of the modulation induced by the back-gate voltage $\beta_{BG,n}$ in the electron doping regime. In other terms, applying a tip bias $V_{tip} = \pm 10$ V has the effect of applying a back-gate voltage of ± 1.6 V relative to the working point. In this limited interval, we can consider I_{sw} as directly proportional to V_{BG} [see inset to Fig. 1(d)]. The same analysis for the hole-doping regime (at $V_{BG} = -10.6$ V) is presented in the supplementary material. Analogous data and analysis from junction J2, reported in the supplementary material, give consistent results.

In Fig. 2(f), we also report results from numerical simulations of the tip-induced modulation. Simulations are performed with a coarse-grained method similar to Ref. 61 that describes the tip potential at the graphene plane with an effective Lorentzian shape.[64,65] Details on the simulations are reported in the supplementary material. Simulation results of the maximum critical current modulation as a function of V_{tip} are reported as red squares in Fig. 2(f) (the term *critical* current refers to simulated results, while *switching* current refers to experimental results). From a linear fit (dashed red line), we obtain $\beta_{simul,n} = 18.0 \pm 1.4$ nA/V, in excellent agreement with the experimental value. In the experimental data points and the simulation in Fig. 2(f), we see a marginal deviation from the linear behavior, following an "s-shape." This feature can be ascribed to the energy-dependence of the barrier at the Nb–graphene interface that is renormalized by the tip potential.[61]

Figures 2(g) and 2(h) show simulated SGM maps for $V_{tip} = -10$ V [Fig. 2(g)] and $V_{tip} = 10$ V [Fig. 2(h)]. The color scale is the same as for the experimental data. Both simulated SGM maps quantitatively reproduce the experimental results and capture all relevant features. Maximum switching current modulation is observed within the junction channel; the modulation decreases toward the junction edge, but is not entirely suppressed when the tip is beyond the junction and located above the Nb contacts.

Interestingly, we note that in Figs. 2(a) and 2(e) the maximum supercurrent modulation is not at the junction center. A stronger switching current reduction is observed on the right in Fig. 2(a), for $V_{tip} < 0$ V [same in Fig. 2(b)], while a stronger enhancement is observed on the left part of the junction in Fig. 2(e). This asymmetry likely arises from a non-uniform electrostatic potential landscape in the junction and highlights the capability of SGM to access information on spatial variations across a superconducting device.

In Fig. 3, we analyze the supercurrent modulation as a function of the distance d for junction J2. An optical microscopy image of J2 is shown in Fig. 3(a). The scanning area of SGM maps is represented by the black square. We report results relative to the n-type doping regime, at $V_{BG} = -3$ V (for J2, $V_{BG}^{CNP} = -7.6$ V) for two different values of V_{tip}. In Fig. 3(b), we report I_{sw} as a function of d for $V_{tip} = -10$ V, while in Fig. 3(c), we report it for $V_{tip} = 10$ V. We present data obtained with two methods: (1) we keep the tip position fixed above the junction center and change only d (red points); (2) we acquire spatial maps, such as those in Figs. 2(a) and 2(e), and extract I_{sw} at the junction center (blue dots). SGM maps of the switching current at $d = 100$ and 300 nm are shown in the insets to Figs. 3(b) and 3(c). The switching current modulation is maximum at minimum distance $d = 100$ nm and rapidly decays when the distance is increased. We observe a reduction of I_{sw} for $V_{tip} < 0$ V and an enhancement for $V_{tip} > 0$ V, as expected from $\beta_{BG,n} > 0$.

In the following, we illustrate an analytical model that accurately reproduces the $I_{sw}(d)$ relationship (all details are reported in the

23 October 2026 16:18:24

© Author(s) 2026

supplementary material). Following Ref. 44, we model the SGM tip as a biased point-like conductive tip placed in front of a conductive plane (graphene). The tip induces a change in the carrier density $\Delta n(x, y)$. Since at the working point ($V_{BG} = -3$ V) I_{sw} can be considered as directly proportional to V_{BG} [and to the charge carrier density $n_{BG} = C_g(V_{BG} - V_{BG}^{CNP})$, where C_g is the back-gate lever arm], it is reasonable to assume that the same linear relationship holds on the local scale as well. This means that the local variation of critical current density $\Delta J_c(x, y)$ is proportional to the local tip-induced variation in carrier density $\Delta n_{tip}(x, y)$. The total critical current is obtained by integrating ΔJ_c over the junction area. We obtain the total critical current as a function of the tip-to-sample distance d_{vac},

$$I_c(d_{vac}) = A \operatorname{arcsinh}\left(\frac{L}{2(d_{vac} + \delta)}\right) + I_{c,0}, \quad (1)$$

where A is a proportionality constant, $\delta = d_{hBN}/\varepsilon_{hBN}$ takes into account the hBN relative dielectric constant $\varepsilon_r = \varepsilon_{hBN}/\varepsilon_0 > 1$ (ε_0 is the vacuum permittivity), and $I_{c,0}$ is the critical current value at large distance d (where the tip has negligible effect). Equation (1) is obtained in the limit of $W \gg L/2, d_{vac}$ and for negligible tip curvature radius. Dashed black lines in Figs. 3(b) and 3(c) were obtained by fitting the red data points to Eq. (1). The fits show a good agreement with the experimental data in the entire range of d. Numerical results of best-fits and data from junction J1 are reported in the supplementary material. The analytical model remains robust in capturing the general $I_{sw}(d)$ dependence also at large d and offers a practical framework for future experiments.

In summary, we performed SGM experiments on GJJs and successfully showed the possibility to locally tune the switching current with the SGM tip. We observed a large switching current modulation of several hundred nA. We studied the switching current modulation as a function of the tip voltage and performed numerical simulations that support our experimental results. In addition, we analyzed how the switching current evolves with tip-to-sample distance, by developing an analytical model that successfully describes the experimental observations.

The switching current modulation obtained in this work is two orders of magnitude larger than in Ref. 61. This was achieved by leveraging the favorable properties of GJJs for SGM investigation. GJJs support larger switching currents up to several μA. This translates not only into a larger (and ambipolar) back-gate modulation efficiency but also into a larger tip-induced switching current tunability. In addition, the larger dielectric constant of hBN increases the capacitive coupling of the tip, further enhancing its effect on the supercurrent. In addition, the use of Nb edge-contacts of the same height as the hBN–graphene–hBN heterostructure allowed us to decrease the working distance from 250 nm (for top contacts)[61] to 100 nm, leading to a relevant enhancement of the tip action. Thanks to this strong tip-induced modulation, we could precisely investigate the effect of the tip at varying distances. A further enhancement of the supercurrent modulation could be obtained by reducing the working distance. In principle, with the optimized geometry of GJJs, it should be possible to work with the tip in contact with the top hBN flake (even though this procedure is extremely challenging due to the proximity of the Nb contacts). This would also result in an increase in the achievable lateral resolution, limited by the top hBN flake thickness and the sharpness of the tip.[61] Our analytical model thoroughly describes the experimental data. Thus, we establish graphene-based Josephson junctions as the ideal platform for spatial investigation of supercurrent transport by SGM.

We note that SGM maps in Figs. 2(a) and 2(e) reveal a slightly asymmetric modulation of the switching current, likely originating from a non-homogeneous electrostatic potential landscape. In Ref. 11, we reported supercurrent rectification in graphene Josephson junctions arising from an asymmetric scattering potential. SGM could be employed not only to spatially investigate the shape of such potential but also as an active tool to locally control it.

In conclusion, this work establishes a robust foundation for advancing SGM on GJJs for precise local mapping of superconducting phenomena, even in combination with magnetic fields, that were previously inaccessible with conventional transport characterization techniques and devices.

See the supplementary material for the additional details, including experimental methods, additional data of the supercurrent modulation as a function of tip bias, SGM maps of junction conductance, additional data on junction J1 in the n-type and p-type doping regimes, additional data on junction J2, details of the numerical simulations, additional data on the supercurrent modulation as a function of tip-to-sample distance, the analytical model for supercurrent modulation as a function of tip-to-sample distance, the connection with the Lorentzian model, and additional data on junction J1 and results of best-fits.

We acknowledge Simone Traverso for useful discussions, and support from projects PRIN2022 2022-PH852L(PE3) TopoFlag and PNRR MUR Project No. PE0000023-NQSTI. K.W. and T.T. acknowledge support from the CREST (No. JPMJCR24A5), JST, and the World Premier International Research Center Initiative (WPI), MEXT, Japan.

AUTHOR DECLARATIONS

Conflict of Interest

The authors have no conflicts to disclose.

Author Contributions

Ivan Villani: Data curation (equal); Formal analysis (equal); Investigation (equal); Software (equal); Validation (equal); Visualization (equal); Writing – original draft (equal); Writing – review & editing (equal). **Samuele Fracassi:** Formal analysis (equal); Methodology (equal); Resources (equal); Software (equal); Validation (equal); Visualization (equal); Writing – review & editing (equal). **Niccolò Traverso Ziani:** Formal analysis (equal); Methodology (equal); Supervision (equal); Validation (equal); Writing – review & editing (equal). **Maura Sassetti:** Conceptualization (equal); Funding acquisition (equal); Methodology (equal); Project administration (equal); Supervision (equal); Validation (equal); Writing – review & editing (equal). **Matteo Carrega:** Conceptualization (equal); Formal analysis (equal); Funding acquisition (equal); Methodology (equal); Resources (equal); Software (equal); Supervision (equal); Validation (equal); Writing – review & editing (equal). **Vaidotas Mišeikis:** Resources (equal). **Camilla Coletti:** Resources (equal). **Fabio Beltram:** Funding acquisition (equal); Resources (equal). **Kenji**

23 October 2026 16:18:24

© Author(s) 2026

Watanabe: Resources (equal). **Takashi Taniguchi:** Resources (equal). **Sergio Pezzini:** Conceptualization (equal); Data curation (equal); Formal analysis (equal); Investigation (equal); Methodology (equal); Supervision (equal); Validation (equal); Writing – review & editing (equal). **Stefan Heun:** Conceptualization (equal); Funding acquisition (equal); Investigation (equal); Methodology (equal); Project administration (equal); Resources (equal); Supervision (equal); Validation (equal); Writing – review & editing (equal).

DATA AVAILABILITY

The data that support the findings of this study are available within the article and its supplementary material.

REFERENCES

[1]M. Tinkham, *Introduction to Superconductivity*, 2nd ed. (McGraw-Hill, New York, 1996).
[2]S. A. Lemziakov, B. Karimi, S. Nakamura, D. S. Lvov, R. Upadhyay, C. D. Satrya, Z.-Y. Chen, D. Subero, Y.-C. Chang, L. B. Wang, and J. P. Pekola, "Applications of superconductor-normal metal interfaces," J. Low Temp. Phys. **217**, 54–81 (2024).
[3]M. Hays, *Realizing an Andreev Spin Qubit* (Springer, 2021).
[4]A. F. Volkov, P. H. C. Magnée, B. J. van Wees, and T. M. Klapwijk, "Proximity and Josephson effects in superconductor-two-dimensional electron gas planar junctions," Physica C **242**, 261–266 (1995).
[5]M. J. Martínez-Pérez, A. Fornieri, and F. Giazotto, "Rectification of electronic heat current by a hybrid thermal diode," Nat. Nanotechnol. **10**, 303–307 (2015).
[6]E. Strambini, F. S. Bergeret, and F. Giazotto, "Proximity nanovalve with large phase-tunable thermal conductance," Appl. Phys. Lett. **105**, 082601 (2014).
[7]J. Wiedenmann, E. Bocquillon, R. S. Deacon, S. Hartinger, O. Herrmann, T. M. Klapwijk, L. Maier, C. Ames, C. Brüne, C. Gould, A. Oiwa, K. Ishibashi, S. Tarucha, H. Buhmann, and L. W. Molenkamp, "4π-periodic Josephson supercurrent in HgTe-based topological Josephson junctions," Nat. Commun. **7**, 10303 (2016).
[8]J. Sarkar, A. Mukherjee, A. Basu, R. Kundu, A. Kundu, and M. M. Deshmukh, "van der Waals Josephson junctions for quantum science and technology," Nat. Rev. Phys. **8**, 619–639 (2026).
[9]B. Turini, S. Salimian, M. Carrega, A. Iorio, E. Strambini, F. Giazotto, V. Zannier, L. Sorba, and S. Heun, "Josephson diode effect in high-mobility InSb nanoflags," Nano Lett. **22**, 8502–8508 (2022).
[10]A. Chieppa, G. Shukla, S. Traverso, G. Bucci, V. Zannier, S. Fracassi, N. Traverso Ziani, M. Sassetti, M. Carrega, F. Beltram, F. Giazotto, L. Sorba, and S. Heun, "Unveiling the current-phase relationship of InSb nanoflag Josephson junctions using a nanoSQUID magnetometer," Nano Lett. **25**, 14412–14419 (2025).
[11]I. Villani, L. Chirolli, M. Carrega, A. Crippa, E. Strambini, F. Giazotto, V. Miseikis, C. Coletti, F. Beltram, K. Watanabe, T. Taniguchi, S. Heun, and S. Pezzini, "Graphene Josephson diodes from inherent asymmetric disorder," arXiv:2606.17673 [cond-mat.supr-con] (2026).
[12]H. B. Heersche, P. Jarillo-Herrero, J. B. Oostinga, L. M. Vandersypen, and A. F. Morpurgo, "Bipolar supercurrent in graphene," Nature **446**, 56–59 (2007).
[13]G. Butseraen, A. Ranadive, N. Aparicio, K. Rafsanjani Amin, A. Juyal, M. Esposito, K. Watanabe, T. Taniguchi, N. Roch, F. Lefloch, and J. Renard, "A gate-tunable graphene Josephson parametric amplifier," Nat. Nanotechnol. **17**, 1153–1158 (2022).
[14]A. W. Draelos, M.-T. Wei, A. Seredinski, H. Li, Y. Mehta, K. Watanabe, T. Taniguchi, I. V. Borzenets, F. Amet, and G. Finkelstein, "Supercurrent flow in multiterminal graphene Josephson junctions," Nano Lett. **19**, 1039–1043 (2019).
[15]F. Telesio, M. Carrega, G. Cappelli, A. Iorio, A. Crippa, E. Strambini, F. Giazotto, M. Serrano-Ruiz, M. Peruzzini, and S. Heun, "Evidence of Josephson coupling in a few-layer black phosphorus planar Josephson junction," ACS Nano **16**, 3538–3545 (2022).
[16]F. Vischi, M. Carrega, A. Braggio, F. Paolucci, F. Bianco, S. Roddaro, and F. Giazotto, "Electron cooling with graphene-insulator-superconductor tunnel junctions for applications in fast bolometry," Phys. Rev. Appl. **13**, 054006 (2020).
[17]E. D. Walsh, W. Jung, G.-H. Lee, D. K. Efetov, B.-I. Wu, K.-F. Huang, T. A. Ohki, T. Taniguchi, K. Watanabe, P. Kim, D. Englund, and K. C. Fong, "Josephson junction infrared single-photon detector," Science **372**, 409–412 (2021).
[18]V. E. Calado, S. Goswami, G. Nanda, M. Diez, A. R. Akhmerov, K. Watanabe, T. Taniguchi, T. M. Klapwijk, and L. M. Vandersypen, "Ballistic Josephson junctions in edge-contacted graphene," Nat. Nanotechnol. **10**, 761–764 (2015).
[19]M. Ben Shalom, M. J. Zhu, V. I. Fal'ko, A. Mishchenko, A. V. Kretinin, K. S. Novoselov, C. R. Woods, K. Watanabe, T. Taniguchi, A. K. Geim, and J. R. Prance, "Quantum oscillations of the critical current and high-field superconducting proximity in ballistic graphene," Nat. Phys. **12**, 318–322 (2016).
[20]F. Amet, C. T. Ke, I. V. Borzenets, J. Wang, K. Watanabe, T. Taniguchi, R. S. Deacon, M. Yamamoto, Y. Bomze, S. Tarucha, and G. Finkelstein, "Supercurrent in the quantum Hall regime," Science **352**, 966–969 (2016).
[21]H. Vignaud, D. Perconte, W. Yang, B. Kousar, E. Wagner, F. Gay, K. Watanabe, T. Taniguchi, H. Courtois, Z. Han, H. Sellier, and B. Sacépé, "Evidence for chiral supercurrent in quantum Hall Josephson junctions," Nature **624**, 545–550 (2023).
[22]J. Barrier, M. Kim, R. K. Kumar, N. Xin, P. Kumaravadivel, L. Hague, E. Nguyen, A. I. Berdyugin, C. Moulsdale, V. V. Enaldiev, J. R. Prance, F. H. L. Koppens, R. V. Gorbachev, K. Watanabe, T. Taniguchi, L. I. Glazman, I. V. Grigorieva, V. I. Fal'ko, and A. K. Geim, "One-dimensional proximity superconductivity in the quantum Hall regime," Nature **628**, 741–745 (2024).
[23]I. Villani, M. Carrega, A. Crippa, E. Strambini, F. Giazotto, V. Mišeikis, C. Coletti, F. Beltram, K. Watanabe, T. Taniguchi, S. Heun, and S. Pezzini, "Quasi-Φ_0-periodic supercurrent at quantum Hall transitions," ACS Nano **19**, 27370–27378 (2025).
[24]S. Jang, G.-H. Park, K. Watanabe, T. Taniguchi, and G.-H. Lee, "Edge dependence of the supercurrent in the quantum Hall regime," Phys. Rev. B **112**, L241401 (2025).
[25]A. Díez-Carlón, M. C. Wuttig, N. Wei, D. Ivanov, P. Altpeter, P. Hakonen, K. Watanabe, T. Taniguchi, L. I. Glazman, and D. K. Efetov, "High-field Josephson effect enabled by a moiré Hofstadter spectrum," arXiv:2607.11721 [cond-mat.mes-hall] (2026).
[26]N. H. Lindner, E. Berg, G. Refael, and A. Stern, "Fractionalizing Majorana fermions: Non-Abelian statistics on the edges of Abelian quantum Hall states," Phys. Rev. X **2**, 041002 (2012).
[27]A. Stern and N. H. Lindner, "Topological quantum computation: From basic concepts to first experiments," Science **339**, 1179–1184 (2013).
[28]D. J. Clarke, J. Alicea, and K. Shtengel, "Exotic non-Abelian anyons from conventional fractional quantum Hall states," Nat. Commun. **4**, 1348 (2013).
[29]J. Alicea and P. Fendley, "Topological phases with parafermions: Theory and blueprints," Annu. Rev. Condens. Matter Phys. **7**, 119–139 (2016).
[30]M. A. Topinka, B. J. LeRoy, S. E. J. Shaw, E. J. Heller, R. M. Westervelt, K. D. Maranowski, and A. C. Gossard, "Imaging coherent electron flow from a quantum point contact," Science **289**, 2323–2326 (2000).
[31]M. A. Topinka, B. J. LeRoy, R. M. Westervelt, S. E. J. Shaw, R. Fleischmann, E. J. Heller, K. D. Maranowski, and A. C. Gossard, "Coherent branched flow in a two-dimensional electron gas," Nature **410**, 183–186 (2001).
[32]B. J. LeRoy, M. A. Topinka, R. M. Westervelt, K. D. Maranowski, and A. C. Gossard, "Imaging electron density in a two-dimensional electron gas," Appl. Phys. Lett. **80**, 4431–4433 (2002).
[33]M. P. Jura, M. A. Topinka, L. Urban, A. Yazdani, H. Shtrikman, L. N. Pfeiffer, K. W. West, and D. Goldhaber-Gordon, "Unexpected features of branched flow through high-mobility two-dimensional electron gases," Nat. Phys. **3**, 841–845 (2007).
[34]M. P. Jura, M. A. Topinka, M. Grobis, L. N. Pfeiffer, K. W. West, and D. Goldhaber-Gordon, "Electron interferometer formed with a scanning probe tip and quantum point contact," Phys. Rev. B **80**, 041303 (2009).
[35]G. J. Percebois, A. Lacerda-Santos, B. Brun, B. Hackens, X. Waintal, and D. Weinmann, "Reconstructing the potential configuration in a high-mobility semiconductor heterostructure with scanning gate microscopy," SciPost Phys. **15**, 242 (2023).

23 October 2026 16:18:24

© Author(s) 2026

[36]C. Gold, B. A. Bräm, R. Steinacher, T. Krähenmann, A. Hofmann, C. Reichl, W. Wegscheider, M. Shayegan, K. Ensslin, and T. Ihn, "Local signatures of electron-electron scattering in an electronic cavity," Phys. Rev. Res. **3**, 013287 (2021).
[37]M. König, M. Baenninger, A. G. Garcia, N. Harjee, B. L. Pruitt, C. Ames, P. Leubner, C. Brüne, H. Buhmann, L. W. Molenkamp, and D. Goldhaber-Gordon, "Spatially resolved study of backscattering in the quantum spin Hall state," Phys. Rev. X **3**, 021003 (2013).
[38]A. Iagallo, N. Paradiso, S. Roddaro, C. Reichl, W. Wegscheider, G. Biasiol, L. Sorba, F. Beltram, and S. Heun, "Scanning gate imaging of quantum point contacts and the origin of the 0.7 anomaly," Nano Res. **8**, 948–956 (2015).
[39]C. Gold, B. A. Bräm, M. S. Ferguson, T. Krähenmann, A. Hofmann, R. Steinacher, K. R. Fratus, C. Reichl, W. Wegscheider, D. Weinmann, K. Ensslin, and T. Ihn, "Imaging signatures of the local density of states in an electronic cavity," Phys. Rev. Res. **3**, L032005 (2021).
[40]B. A. Braem, F. M. Pellegrino, A. Principi, M. Röösli, C. Gold, S. Hennel, J. V. Koski, M. Berl, W. Dietsche, W. Wegscheider, M. Polini, T. Ihn, and K. Ensslin, "Scanning gate microscopy in a viscous electron fluid," Phys. Rev. B **98**, 241304 (2018).
[41]M. Huefner, B. Kueng, S. Schnez, K. Ensslin, T. Ihn, M. Reinwald, and W. Wegscheider, "Spatial mapping and manipulation of two tunnel-coupled quantum dots," Phys. Rev. B **83**, 235326 (2011).
[42]B. Brun, N. Moreau, S. Somanchi, V.-H. Nguyen, K. Watanabe, T. Taniguchi, J.-C. Charlier, C. Stampfer, and B. Hackens, "Imaging Dirac fermions flow through a circular Veselago lens," Phys. Rev. B **100**, 041401 (2019).
[43]C. Gold, A. Kurzmann, K. Watanabe, T. Taniguchi, K. Ensslin, and T. Ihn, "Scanning gate microscopy of localized states in a gate-defined bilayer graphene channel," Phys. Rev. Res. **2**, 043380 (2020).
[44]B. Brun, N. Moreau, S. Somanchi, V.-H. Nguyen, A. Mrenca-Kolasinska, K. Watanabe, T. Taniguchi, J.-C. Charlier, C. Stampfer, and B. Hackens, "Optimizing Dirac fermions quasi-confinement by potential smoothness engineering," 2D Mater. **7**, 025037 (2020).
[45]B. Brun, V.-H. Nguyen, N. Moreau, S. Somanchi, K. Watanabe, T. Taniguchi, J.-C. Charlier, C. Stampfer, and B. Hackens, "Graphene whisperitronics: Transducing whispering gallery modes into electronic transport," Nano Lett. **22**, 128–134 (2022).
[46]M. D. Petrovic, S. P. Milovanovic, and F. M. Peeters, "Scanning gate microscopy of magnetic focusing in graphene devices: Quantum versus classical simulation," Nanotechnology **28**, 185202 (2017).
[47]K. E. Aidala, R. E. Parrott, T. Kramer, E. J. Heller, R. M. Westervelt, M. P. Hanson, and A. C. Gossard, "Imaging magnetic focusing of coherent electron waves," Nat. Phys. **3**, 464–468 (2007).
[48]S. Bhandari, G.-H. Lee, A. Klales, K. Watanabe, T. Taniguchi, E. Heller, P. Kim, and R. M. Westervelt, "Imaging cyclotron orbits of electrons in graphene," Nano Lett. **16**, 1690–1694 (2016).
[49]S. Bhandari, G. H. Lee, K. Watanabe, T. Taniguchi, P. Kim, and R. M. Westervelt, "Imaging electron flow from collimating contacts in graphene," 2D Mater. **5**, 021003 (2018).
[50]N. Paradiso, S. Heun, S. Roddaro, L. N. Pfeiffer, K. W. West, L. Sorba, G. Biasiol, and F. Beltram, "Selective control of edge-channel trajectories by scanning gate microscopy," Physica E **42**, 1038–1041 (2010).
[51]N. Paradiso, S. Heun, S. Roddaro, D. Venturelli, F. Taddei, V. Giovannetti, R. Fazio, G. Biasiol, L. Sorba, and F. Beltram, "Spatially resolved analysis of edge-channel equilibration in quantum Hall circuits," Phys. Rev. B **83**, 155305 (2011).
[52]N. Paradiso, S. Heun, S. Roddaro, G. Biasiol, L. Sorba, D. Venturelli, F. Taddei, V. Giovannetti, and F. Beltram, "Imaging backscattering through impurity-induced antidots in quantum Hall constrictions," Phys. Rev. B **86**, 085326 (2012).
[53]N. Paradiso, S. Heun, S. Roddaro, L. Sorba, F. Beltram, G. Biasiol, L. N. Pfeiffer, and K. W. West, "Imaging fractional incompressible stripes in integer quantum Hall systems," Phys. Rev. Lett. **108**, 246801 (2012).
[54]L. Bours, S. Guiducci, A. Mreńca-Kolasińska, B. Szafran, J. C. Maan, and S. Heun, "Manipulating quantum Hall edge channels in graphene through scanning gate microscopy," Phys. Rev. B **96**, 195423 (2017).
[55]K. Kaperek, S. Heun, M. Carrega, P. Wójcik, and M. P. Nowak, "Theory of scanning gate microscopy imaging of the supercurrent distribution in a planar Josephson junction," Phys. Rev. B **106**, 035432 (2022).
[56]S. Maji, K. Sowa, and M. P. Nowak, "Scanning gate microscopy of nonretracing electron-hole trajectories in a normal-superconductor junction," Phys. Rev. B **109**, 115410 (2024).
[57]S. Maji and M. P. Nowak, "Aharonov-Bohm interference probing of chiral Andreev edge states via scanning gate microscopy," arXiv:2609.27716 [cond-mat.mes-hall] (2026).
[58]M. Huefner, C. May, S. Kicin, K. Ensslin, T. Ihn, M. Hilke, K. Suter, N. F. de Rooij, and U. Staufer, "Scanning gate microscopy measurements on a superconducting single-electron transistor," Phys. Rev. B **79**, 134530 (2009).
[59]M. Hegedüs, R. Banerjee, A. Hutcheson, T. Barker, S. Mahashabde, A. V. Danilov, S. E. Kubatkin, V. Antonov, and S. E. de Graaf, "*In situ* scanning gate imaging of individual quantum two-level system defects in live superconducting circuits," Sci. Adv. **11**, eadt8586 (2025).
[60]S. Bhandari, G.-H. Lee, K. Watanabe, T. Taniguchi, P. Kim, and R. M. Westervelt, "Imaging Andreev reflection in graphene," Nano Lett. **20**, 4890–4894 (2020).
[61]A. Lombardi, G. Shukla, G. Bucci, S. Salimian, V. Zannier, S. Traverso, S. Fracassi, N. Traverso Ziani, M. Sassetti, M. Carrega, F. Beltram, L. Sorba, and S. Heun, "Supercurrent modulation in InSb nanoflag-based Josephson junctions by scanning gate microscopy," Commun. Mater. **6**, 272 (2025).
[62]V. Miseikis, D. Convertino, N. Mishra, M. Gemmi, T. Mashoff, S. Heun, N. Haghighian, F. Bisio, M. Canepa, V. Piazza, and C. Coletti, "Rapid CVD growth of millimetre-sized single crystal graphene using a cold-wall reactor," 2D Mater. **2**, 014006 (2015).
[63]S. Pezzini, V. Mišeikis, S. Pace, F. Rossella, K. Watanabe, T. Taniguchi, and C. Coletti, "High-quality electrical transport using scalable CVD graphene," 2D Mater. **7**, 041003 (2020).
[64]B. Szafran, "Scanning gate microscopy simulations for quantum rings: Effective potential of the tip and conductance maps," Phys. Rev. B **84**, 075336 (2011).
[65]E. D. Herbschleb, R. K. Puddy, P. Marconcini, J. P. Griffiths, G. A. Jones, M. Macucci, C. G. Smith, and M. R. Connolly, "Direct imaging of coherent quantum transport in graphene $p-n-p$ junctions," Phys. Rev. B **92**, 125414 (2015).

23 October 2026 16:18:24

© Author(s) 2026